Process Recipes for Additively Printed Copper-Ink Flexible Circuits using Direct Write Methods

Pradeep Lall
Auburn University
NSF-CAVE3 Electronics Research Center
Department of Mechanical Engineering
Auburn, AL 36849
E-mail: lall@auburn.edu;
Tele: +1(334)844-3424

Jinesh Narangaparambil
Auburn University
NSF-CAVE3 Electronics Research Center
Department of Mechanical Engineering
Auburn, AL 36849

Kyle Schulze
Auburn University
NSF-CAVE3 Electronics Research Center
Department of Mechanical Engineering
Auburn, AL 36849

Curtis Hill
Jacobs Space Exploration Group | Quantitech
NASA Marshall Space Flight Center
Huntsville, AL

***Abstract* – In this paper, the process-recipes and process-performance relationships for additive-printing of copper circuits using direct-write methods have been studied. The process has been implemented on the direct write platform. Interest in the use of additive printing methods for the manufacture of micro-circuits has grown immensely in recent times. Direct write methods have been shown to have the ability to create circuits in a limited manner. However, the process recipes and the effect of process parameters on the manufactured properties are not well understood. Copper ink is a good and cost-effective alternative to silver ink but its use has lagged owing to an increased propensity for oxidation. In this paper, photonic curing has been used to sinter copper ink to make the traces conductive. The method flashes high energy light that sinter metal particles instantaneously and the temperature of the substrate remains low. The effect of the different photonic sintering profiles on the mechanical and electrical properties of the printed traces has been studied in this paper. The print process parameters also play an important role in the line width and height that has been studied to print with the desired line profile for the end application. An LC filter circuit is been printed with SMD components been attached using an electrically conductive adhesive (ECA). The manufactured flexible LC filter is been tested for its frequency sweep to compare with the commercially available LC filer with the help of the Bode plot.**

***Keywords* –** Direct-Write, Additive printing, Flexible electronics, Polyimide, Copper ink, Photonic sintering, Electrically Conductive Adhesive.

Nomenclature

Cu	Copper
ECA	Electrically Conductive Adhesive
AM	Additive Manufacturing
SLF	Shear Load to Failure

I. INTRODUCTION

Flexible electronics is an alternative to conventional print-and-etch electronics in emerging applications such as flexible display, wearable sensors, removable RFID tags, flexible battery, e-skin, etc. Continuous efforts to minimize traditional form considerations in terms of size and weight has added the need for foldable electronic products for portability. Flexible electronics have the desired ability to fold, flex, stretch and twist. Wearable electronic applications including sports and recreation, healthcare, military and defense clothing, lifestyle, consumer electronics, offer opportunities for integration of electronics circuits on pliable non-traditional substrates [[1], [2]]. A number of different platforms are available in the additive manufacturing (AM), including Aerosol Jet, Inkjet and Micro-Dispensing. This paper focuses on the direct write micro-dispensing method. The technology used for this paper's results is from the standard direct write technology. This system has numerous benefits over other printing systems, such as the handling of viscosities ranging from 1 cps to several million cps [[6]]. This opens up a wide variety of possibilities in the electronics industry, such as printing of ECAs, solders, conductive inks, etc.

The relationship between microstructure of the printed components including particle growth and porosity, and electrical conductivity during post-heat treatment has been previously studied [[7], [8]]. Various sintering processes have been developed, such as conventional thermal sintering, laser sintering, UV sintering, plasma sintering and microwave sintering. Photonic sintering often referred to as flash-light sintering has the advantage of being able to be done at room temperature under ambient conditions at ultra-fast speed. This merit plays an important role in the scaling-up processes for printed copper. The effect of the different parameters in photonic curing has not been previously investigated. Photonic curing offers the promise of minimizing damage to the substrate, such as PI and PET, during the process compared to other processes. Photonic sintering becomes more important when sintering a copper ink as copper tends to oxidize in the ambient state and requires an inert sintering condition that can be overcome by using Photonic sintering.

In this paper, a number of different process parameters related to copper ink printing have been examined. Process scale-up for high volume production requires data on the correlation of the process parameters with the electrical and mechanical performance of the printed circuits. The study is

divided into four parts: (a) Print process development (b) Photonic sintering method (c) Establish component interconnection and (c) Final application by printing LC filters. Various parameters that affect printing processes include ink pressure, stage speed, stand-off height, nozzle diameter, and substrate [[4], [5]]. The variance in the geometry of the profile is associated with the mechanical and electrical properties. The electrical and mechanical properties are both related to the sintering process state, which has also been studied at the same time. There are iterative methods. Photonic sintering plays an equally significant role in this study. The effect of different recipe parameters for photonic sintering is energy, number of flashes, on time, off time, frequency/period and flash mode (i.e. burst mode or continuous mode) with different stage speed. The finalized parameters are then used to reproduce a commercially obtained LC filter. The conventional rigid LC filter performance is then compared to the flexible printed LC filter using the Bode plot.

II. Test Vehicle Design

The test vehicle has been designed and manufactured at CAVE3 electronics research center. The flexible substrate used in this test vehicle is polyimide. The polyimide substrate is 5mil in thickness which are plasma cleaned for 5minutes at 100W, O_2 clean. The polyimide film sustains a temperature of 300˚C. The direct-write technique is been used for printing. The system has four printing heads which include two Smart pumps and two nFD pumps. The data reported in this paper is for the Smart Pumps. The nozzle used to dispense the silver ink and ECA has a nozzle diameter of ID/OD - 0.159/0.244µm respectively. The nozzle is a Luer adapter nozzle. The standoff height for the printing is 0.05mm.

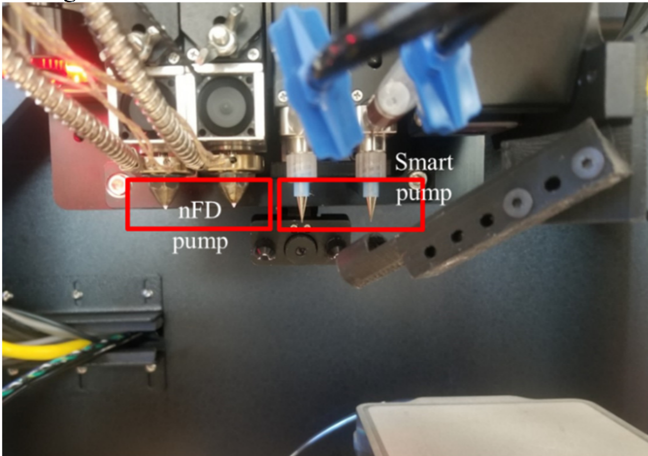

Figure 1: nFD and Smart pump set up on the system

A. Ink Properties:

1) Conductive (Copper) ink

The copper (Cu) ink is compatible with substrates like paper, plastics, glass, and fabrics. The ink is a photonic sinterable. The copper ink has a viscosity in range of 25,000cP and density of 3.1g/ml.

Table 1: Conductive Ink properties

Parameters	Value
Viscosity	25,000cP-30,000cP at 50 sec^{-1}
Density	3.1 g/ml
Solid Content	82 wt%
Sheet resistivity	10mΩ/sq/mil

2) ECA ink

The ECA ink has a recommended curing condition of 150˚C. The ECA used is compatible with silver and copper-based conductive inks. The ECA ink viscosity changes with the change in shear-rate. The ink viscosity is in the range of 15,000cP to 110,000cP depending on the shear rate imposed. The specific gravity of the ECA ink is 3.2.

Table 2: ECA Ink properties

Parameters	Value
Viscosity	110,000cP at 1 sec^{-1} 30,000cP at 10 sec^{-1} 15,000cP at 100 sec^{-1}
Specific gravity	3.2
Tg	-10˚
Volume Resistivity	< 9 x 10^5 Ω*cm

B. Test Vehicle design – 1

The test vehicle design - 1 is for the print process study and the sintering profile study. Each condition is been replicated in the form of 5 lines with pads at both ends.

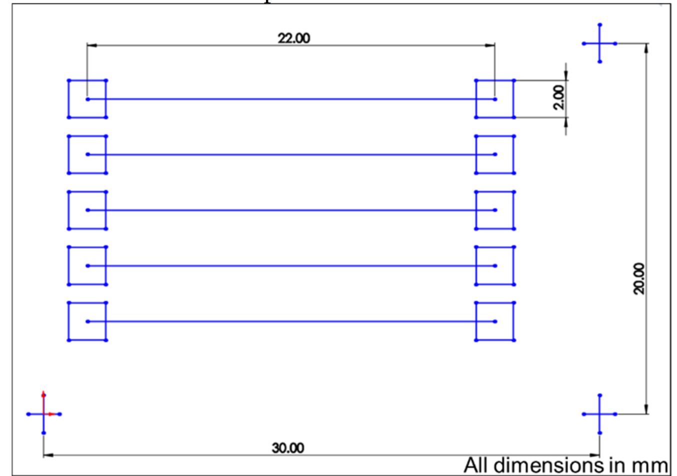

Figure 2: Test vehicle design – 1

Figure 2 shows the test vehicle used for the process and sintering study in this paper. Each test vehicle has 5 traces with pads at both ends. The number of traces are 5 in order to check for the consistency of the printing at a set process parameter. Each test condition is run three times to calculate the variation.

1) Print Process study

Cu ink has been studied for various process parameters, such as printing speed and ink pressure, for good print quality. The good quality print parameter includes consistent ink deposition with a clean trace definition. Mechanical properties and electrical properties have been studied in accordance with the process parameters of the profile variation (trace height and width). In this case, the mechanical and electrical properties would be in coordination with the cross-section area.

Table 3: Various Print process parameters

Parameters	Variation
Print speed	1mm/s 3mm/s 5mm/s

	10mm/s
Ink pressure	10psi 15psi 18psi 25psi

2) Sintering study

Sintering profile plays an important role in the mechanical and electrical properties which are also been reported in the prior work [[11]]. The effect on shear load to failure and resistance is a very important factor after having a defined trace being printed after the print process study.

Table 4: Various sintering conditions

Parameters	Variation
Sintering conditions	Energy Frequency Stage speed of the photonic system

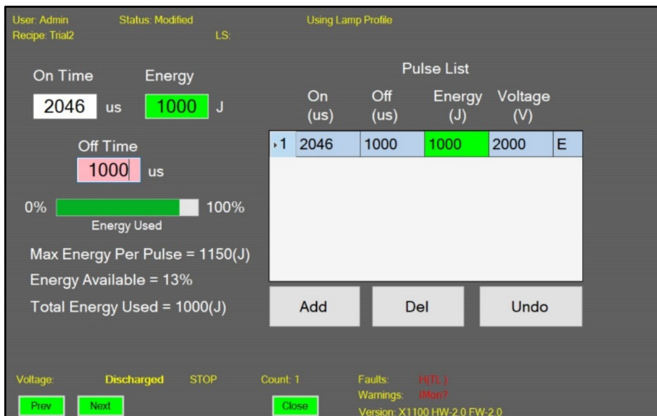

Figure 3: Photonic curing system Lamp profile

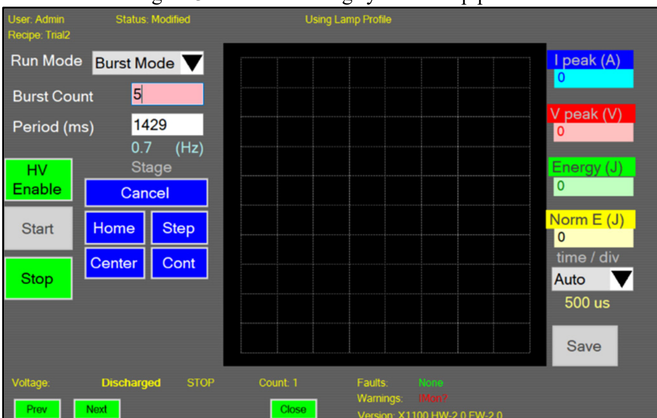

Figure 4: Curing Burst-Run mode setup screen

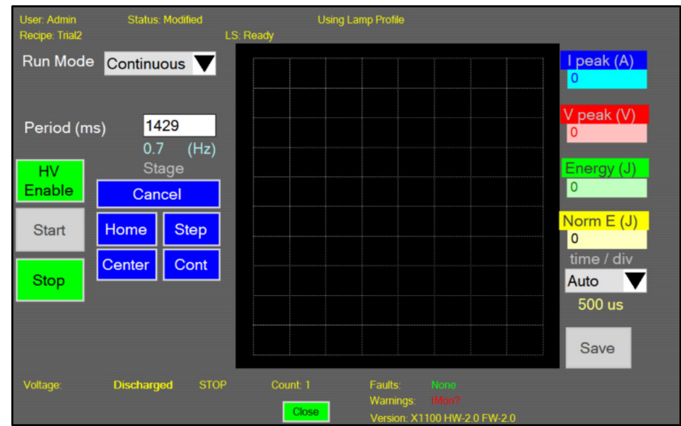

Figure 5: Curing Continuous-Run Mode setup screen

Figure 3-Figure 5 shows the lamp profile screen with various parameters for the setup of the curing profile. There are not many studies showing the effect of each of these parameters on the printed traces.

Definition of the notations from the system that are the variables to find an optimized photonic sintering recipe. (From the Xenon manual):

Voltage – Voltage value defines the maximum and peak energies for the cure. Maximum voltage - 3000V

Energy – Energy for the pulse in the sequence. It's inter-related with On Time.

Off Time – which is the time between the current pulse and the next pulse in the sequence.

Run Mode – determines how many times and at what frequency the pulse sequence will repeat. The user selects from three options:

1. Single: the pulse sequence runs once and stops automatically.
2. Burst: the pulse sequence repeats a finite number of times and stops automatically.
3. Continuous: the pulse sequence repeats infinitely until manually stopped by the user.

Stage Speed – Defines the stage travel speed during the pulse flashing

Step size – Defines the forward move, thus can be related to flash energy overlap.

The ECA has a recommended curing condition of 150˚C for 30mins.

C. Test Vehicle Design – 2

The test design – 1 gives a final print process parameters with the optimized sintering condition for the particular silver ink. These optimized parameters are used for further study. The design 2 is to verify the functionality of the ECA material in establishing the interconnection between the passive components and the printed conductive traces. This design is to compare the measured values against the rated values of the commercially available components like a resistor (R), capacitor (C) and an inductor (L).

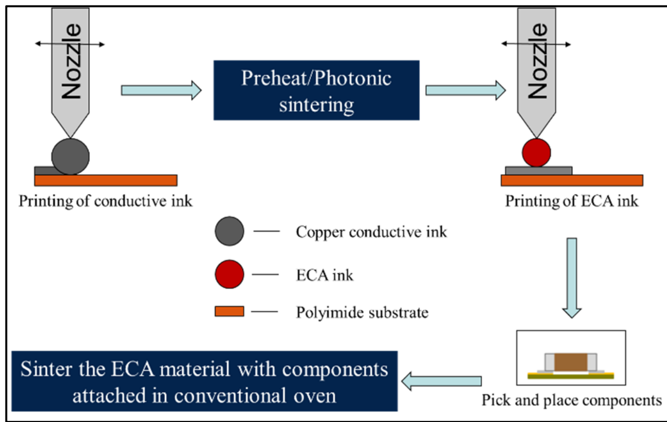

Figure 6: Process flow for component attachment

Figure 6 indicates the process flow for the connection of the parts. The polyimide substrate used in this study was initially cleaned from plasma and then attached to the stage. The conductive ink (Layer 1) is printed and then cured using flash curing. Post curing, the sample is transferred to the stage and fiduciary matching is accompanied by ECA ink printing (Layer 2). After the ECA has been printed, the components are picked and placed on the ECA printed pads and then cured in the oven at the recommended temperature. The test vehicle board size specification complies with the ASTM standards.

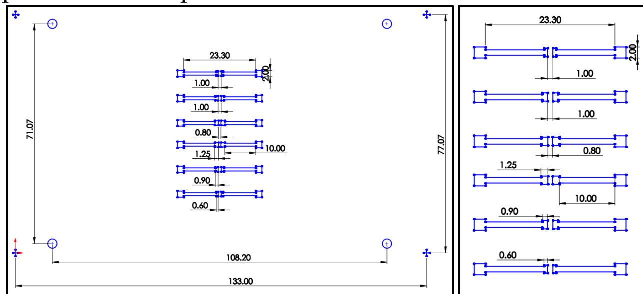

Figure 7: Layer 1(Conductive Ink) Design for Test Vehicle Design-2 with zoomed in view

Layer 1 is been printed at a standoff height of 0.050mm which is for the conductive traces. Layer 2 is been printed at a standoff height of 0.080 from the polyimide surface. The standoff height is been increased considering the trace height from Layer 1.

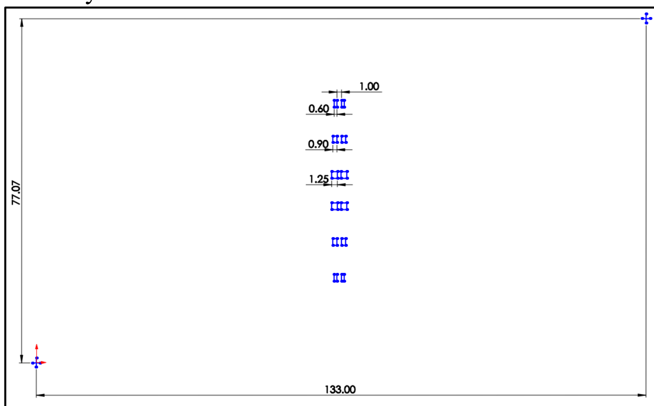

Figure 8: Layer 2(ECA) Design for Test Vehicle Design-2

Table 5: Specification of the discrete components

Components	Code	Rated value	Dimension (L X W X H)
Resistor	0805(2012 Metric)	1kOhms	2.00mm x 1.25mm x 0.60mm
Capacitor	0805(2012 Metric)	1.8pF @ 7.96 MHz	2.00mm x 1.25mm x 0.70mm
Inductor	0806(2016 Metric)	2.2uH @ 1 kHz	2.00mm x 1.25mm x 1.80mm

Table 5 contains descriptions of the components used in the test vehicle – 2. Tin is the material at the terminal of the components.

D. Test vehicle Design – 3

The design 3 is the LC filter design that will be our application demo from the study we have done with the test vehicle 1 and 2. The LC filter design is similar to a commercially available LC filter. The printed flexible LC filter is compared to a commercially bought LC filter. The components attached are of the same ratings as on the commercially bought filter. Both the filters would be tested for its performance and compared with the help of the Bode plot.

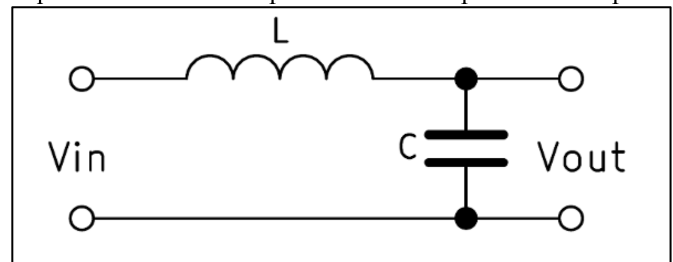

Figure 9: Schematic circuit diagram for the LC filter

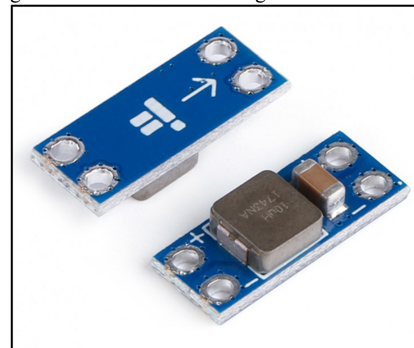

Figure 10: Commercially procured LC filter

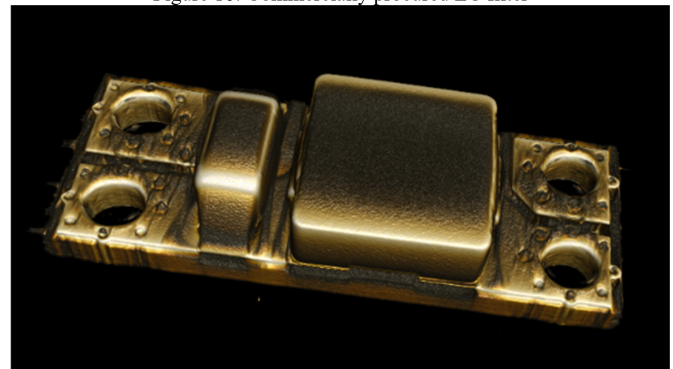

Figure 11: CT scan image of the commercial LC filter

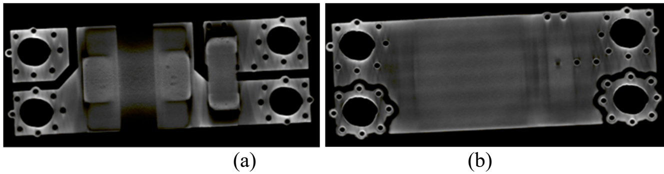

(a) (b)

Figure 12: CT scan image of LC filter (a) Top Layer (b) Bottom Layer

The design for the flexible LC filter was been made using these images that were been captured using the CT scan machine shown in Figure 11 and Figure 12.

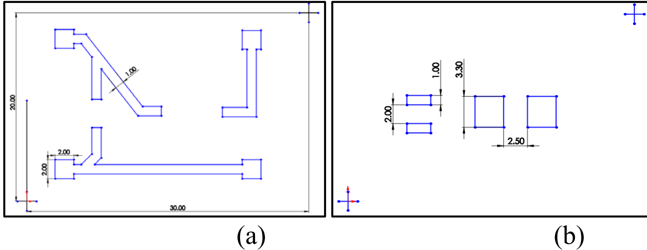

(a) (b)

Figure 13: Design for Test Vehicle Design-3 (a) Layer 1(Conductive Ink) (b) Layer 2(ECA)

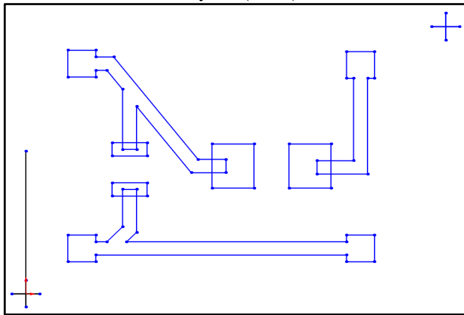

Figure 14: Overlapping of Layer 1 and Layer 2 for Test Vehicle Design-3

Figure 13 and Figure 14 shows the test vehicle for design 3. The test pattern is replicated according to the actual LC filter board shown in Figure 10.

III. Test Results And Discussion

All the dimensions reported during the analysis is an average value of 5 samples. In this section, the effect of various process parameters on the print consistency, mechanical and electrical properties has been examined. White-light interferometry is used for print consistency measurements.

A. Test results from the design-1

1) Effect of Various Print speeds on Print Profile

The following process parameters are constant for the printing: (a) Ink Pressure = 18 psi (b) Standoff height = 0.05mm (c) Number of passes = 1. All the optical Images are been captured at the same magnification for comparison.

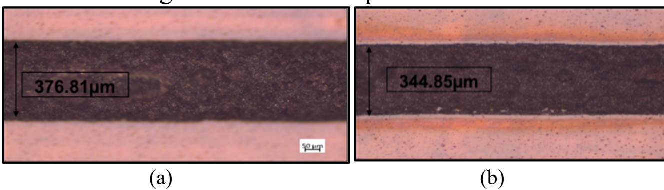

(a) (b)

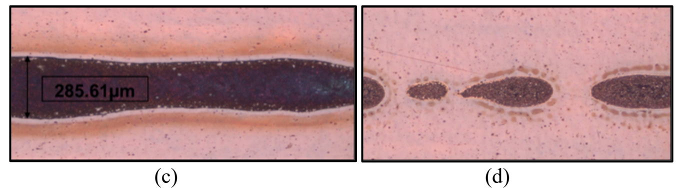

(c) (d)

Figure 15: Trace width with a print speed of (a) 1mm/s, (b) 3mm/s, (c) 5mm/s, (d) 10mm/s

Figure 15 demonstrate the difference in the width of the trace due to the change in printing speed. Print consistency keeps deteriorating and at 5mm/s we can see that we don't get a consistent trace width, thus defines the peak speed limit. The measurement of white light interferometry is conducted using the Bruker Contour GT-K machine. The surface of the polyimide is normalized to form the base of the surface. the repeatability of the print from the multiple printed samples. The test vehicle consists of 5 traces and we print 3 test vehicles at each condition at different days that cumulates to 15 traces been analyzed. Figure 16, demonstrates the variance of the trace profile due to various print speed. To demonstrate the repeatability of the print, we attempted to examine the trace height of two traces simultaneously. It can be found that print quality and geometry are consistent and repeatable. The figures consists of the white light interferometry analysis with its cross-sectional profile plotted in the graph. Trace heights can be measured and it can be seen that with the increased speed, the time required for filing decreases the efficiency of the printing by giving a waved printing. It also resembles that it decreases the cross-section area with increased speed due to lower mass deposition per unit travel as expected.

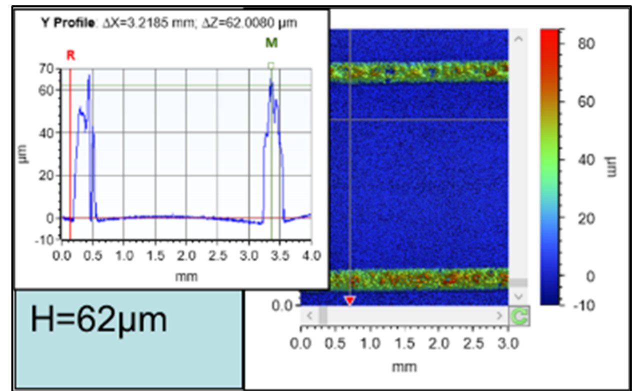

(a)

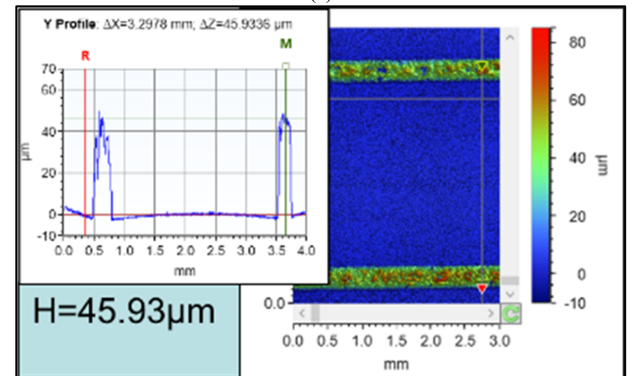

(b)

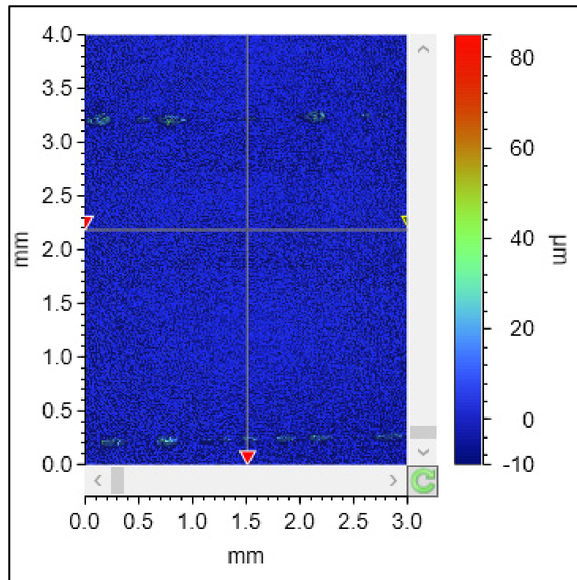

(c)

Figure 16: Trace profile and Height with a print speed of (a) 1mm/s, (b) 3mm/s, (c) 10mm/s

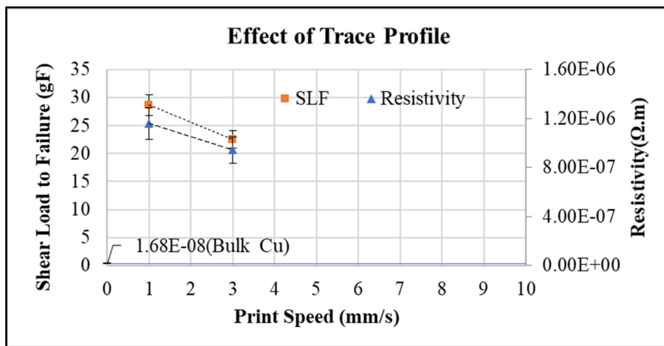

Figure 17: Effect of various trace profile due to print speed on SLF and resistivity

Figure 17, demonstrate the mechanical and electrical properties of traces of varying geometry profiles at different printing speeds. If the speed increases, the cross-sectional geometric measurements decrease and hence the resistivity and shear load to the failure values.

2) Effect of the various ink pressure

The following process parameters are constant for the printing: (a) Print speed = 3mm/s (b) Standoff height = 0.05mm (c) Number of passes = 1. All the optical Images are been captured at the same magnification for comparison.

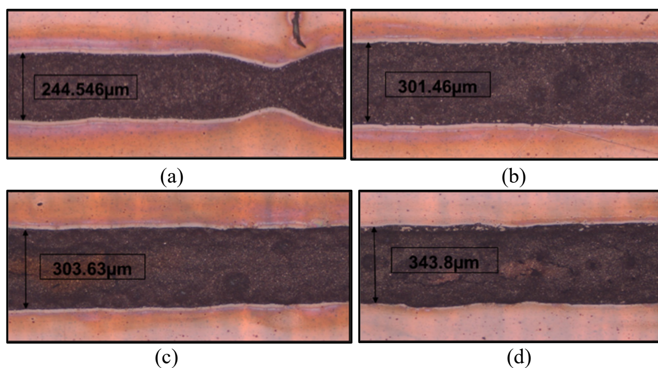

(a) (b) (c) (d)

Figure 18: Trace width for ink pressure of (a) 10 psi, (b) 15psi, (c) 18psi, (d) 25psi

Figure 18, shows the trace width variation due to the change in the pressure of the ink. Trace width tends to increase with increased ink pressure due to increased mass flow rate, but a certain cap of ink pressure cannot be exceeded provided the viscosity of the ink, controlled material dispense [10] and the components in the system. Thus the pressure of the ink may be set based on the print specification and the trace width criterion. Figure 19, shows the trace profile variation. It can be observed that the print quality and geometry is consistent over the various prints. The print speed and the ink pressure thus can be used a two counter-correcting variables. Higher print speeds reduce the line width as shown previously. In contrast, higher ink pressures increase the line width. In a real process, to reduce the throughput time, a process engineer may select a higher print speed allowable and then select the pressure needed to achieve the required line width. The increase in ink pressure also increases the line height as shown in Figure 19 for the ink pressures in the range of 10psi to 25 psi.

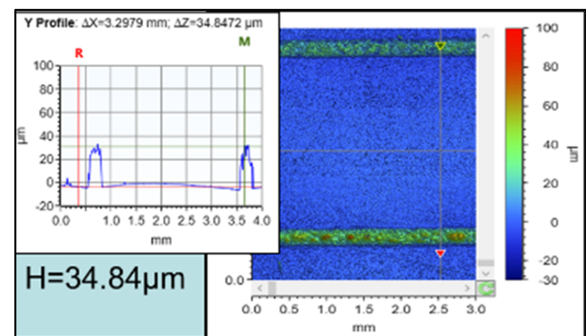

(a)

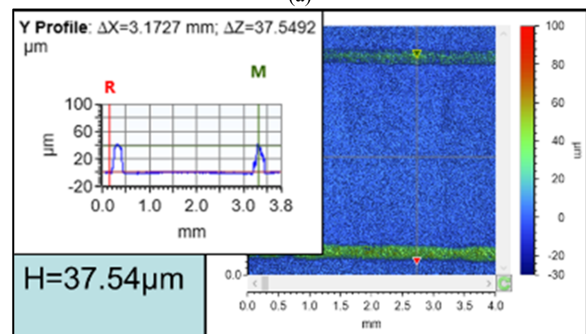

(b)

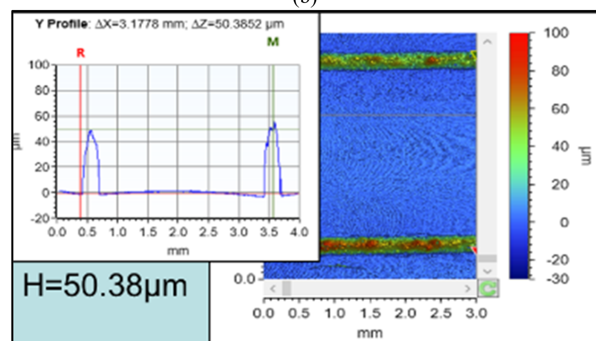

(c)

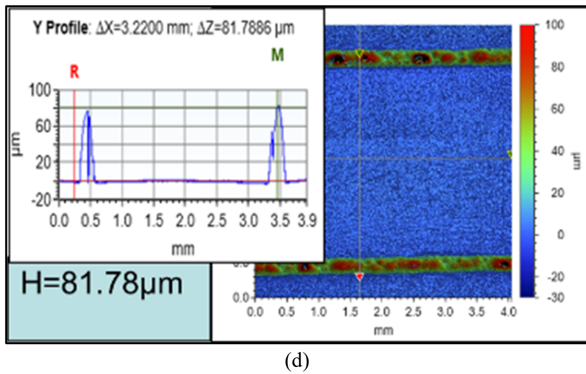

(d)

Figure 19: Trace profile and Height with ink pressure of (a) 10 psi, (b) 15psi, (c) 18psi, (d) 25psi

Figure 20, shows the mechanical and electrical properties of the traces with various geometry profile from the various ink pressure. Data from Figure 17 and Figure 20 helps in understanding the ink behavior and finalizing the process parameters for better mechanical and electrical properties. From the two process conditions (printing speed and ink pressure) the effect of the cross-section area is plotted against the electrical and mechanical properties in Figure 21 and Figure 22. The cross-section area is considered to be parabolic. It can be observed that with the rise in the cross-section area, the resistivity, and the shear load to failure increases.

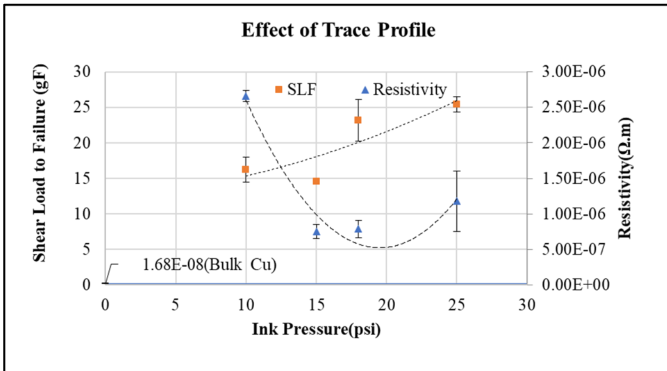

Figure 20: Effect of various trace profile due to ink pressure on SLF and resistivity

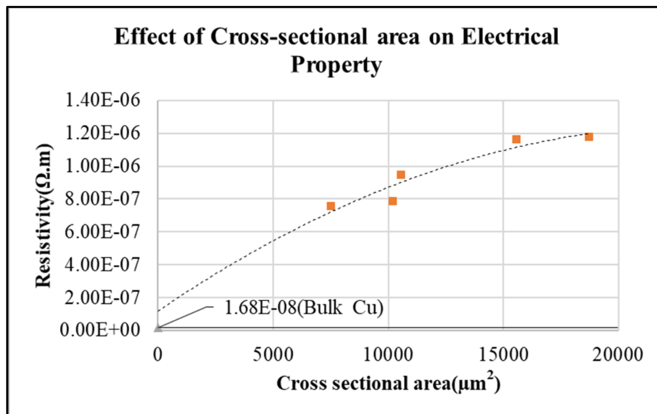

Figure 21: Effect of varying cross-sectional area on the resistance

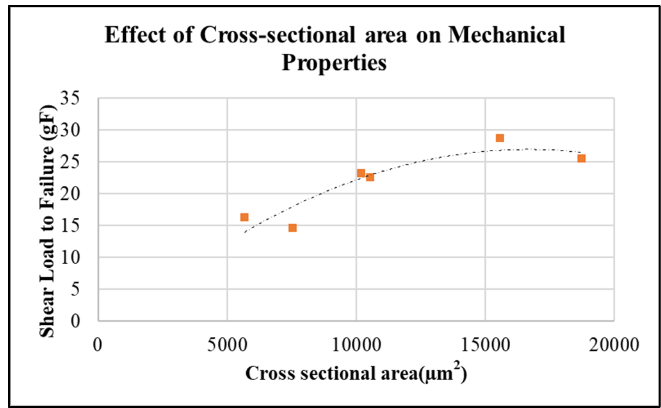

Figure 22: Effect of varying cross-sectional area on the shear load to failure

The data from print speed and ink pressure combined with its effect on cross-sectional area which ultimately effects the electrical and mechanical properties gives a summary to selection of the print process parameters with same sintering conditions.

3) Effect of Various Photonic sintering conditions

There are various parameters to be considered in the photonic sintering. Each parameter variation tends to define the amount of cure. The aperture size for the system is set to be 80mm which is the maximum slit size. The aperture size is kept constant over the whole study in this paper.

a) Effect of Flash energy

The traces were printed with one pass and then been sintered with varying energy of the flash. For the particular testing the following parameters were set as constant: Total Voltage = 2000V; Frequency = 0.7 Hz; the sintering was performed under the Burst mode, number of bursts = 5

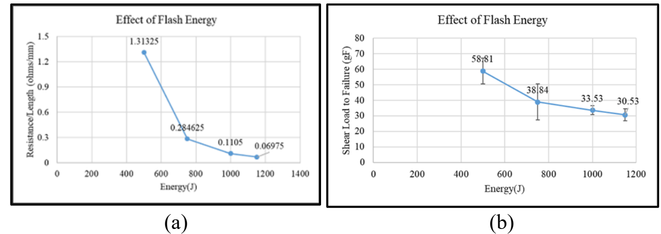

(a) (b)

Figure 23: Effect of flash energy (a) Resistance/length (b) Shear load to failure

From Figure 23, it can be observed that with increasing the flash energy for a set voltage, the resistance per unit length decreases and the shear load to failure values increases.

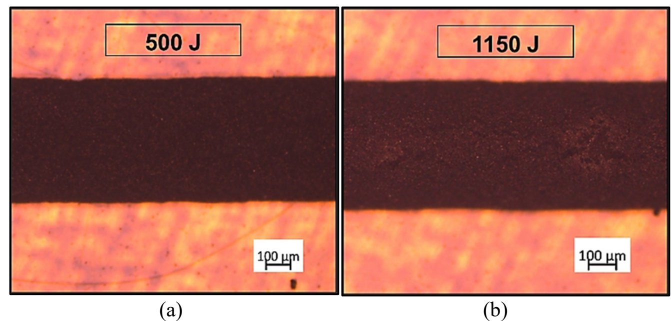

(a) (b)

Figure 24: Optical image of the surface at various flash energy

From Figure 24, it can be seen that the 1000J samples tend to develop a popcorn type of failure where we see cracks on the surface as seen in Figure 24(b). The reason for the popcorn type failure would be due to the entrapped solvent content receiving high temperature at an instantaneously small amount of time forcing it to evaporate forming voids in the trace.

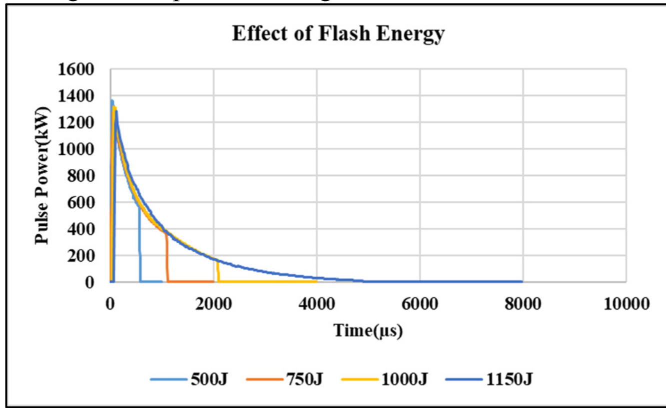

Figure 25: Pulse profile for various flash energy

Figure 25 shows the pulse power available at the substrate during the flash. It can be observed that with increase in flash energy at constant pulse power the amount of time the energy available is also higher. Thus, mentioning that the exposure time of the samples is higher with higher energy.

b) *Effect of Varying Frequency*

The frequency plays an important role when sintering bigger sized samples. The parameters that were set constant for this test are: (a) Total Voltage = 2000V (b) Energy = 1000J (c) The sintering was performed under the Burst mode, thus Number of bursts = 5

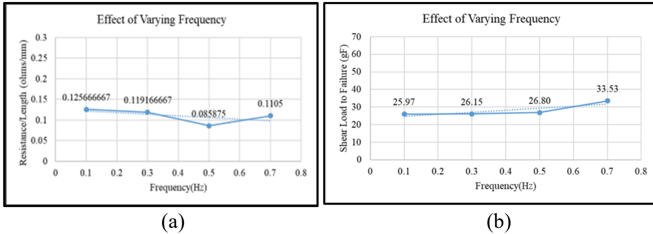

(a) (b)

Figure 26: Effect of flash frequency (a) Resistance/length (b) Shear load to failure

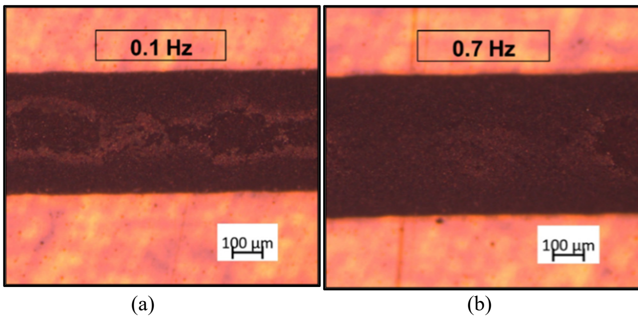

(a) (b)

Figure 27: Optical image of the surface at various frequency

Figure 26 shows us the effect of the varying frequency. Increasing frequency means decreasing period and thus the same amount of energy is been dissipated in a shorter duration. Ideally, with higher frequency the amount of cure should be better as the flashes of energy is at a faster rate which may help in the conductive particles to agglomerate. From Figure 27, it can also be seen that there is a popcorn failure occurring which tends to show that the amount of energy provided is higher and traces tend to burn. 0.1 Hz and 0.7 Hz being the minimum and maximum frequency available for the defined total energy. There is not much variation in the electrical and mechanical properties.

c) *Effect of Varying Off-Time*

In the current study we are sintering with only one define pulse recipe, thus the variation in the electrical and mechanical properties should be negligible. The parameters that were set constant for this test are: Total Voltage = 2000V (b) Energy = 1000J (c) Frequency = 0.7Hz. The sintering was performed under the Burst mode, thus Number of bursts = 5

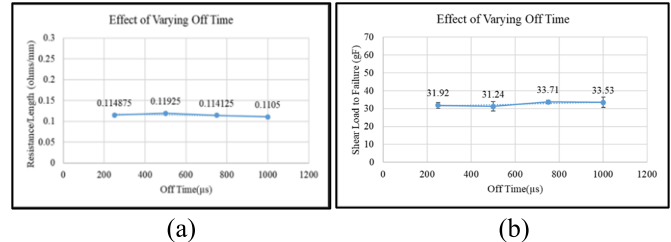

(a) (b)

Figure 28: Effect of Off-time (a) Resistance/length (b) Shear load to failure

Figure 28, shows no variation in the electrical and mechanical properties as the off-time variable is only applicable when there are multiple energy pulses. Figure 29, shows similar cure condition for the mentioned off-times.

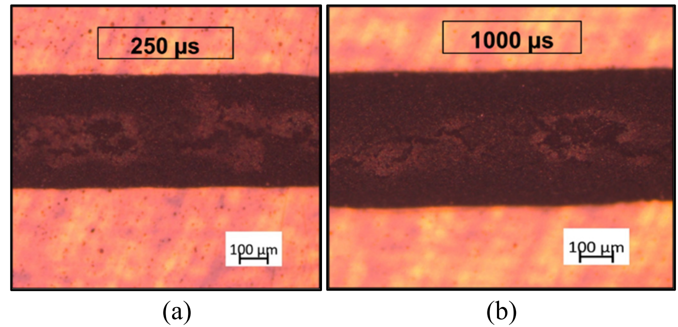

(a) (b)

Figure 29: Optical image of the surface at various Off Time

d) *Effect of Varying Stage speed*

The system has a moving stage that can be used to set a stage speed and frequency in order to sweep bigger sized samples with equal amount of energy been provided per unit surface area. With varying speed and with constant frequency the percentage of overlap would vary thus changing the amount of energy that is been focused at a particular point on the test vehicle. With increasing speed the overlap percentage would reduce thus the amount of cure would also change.

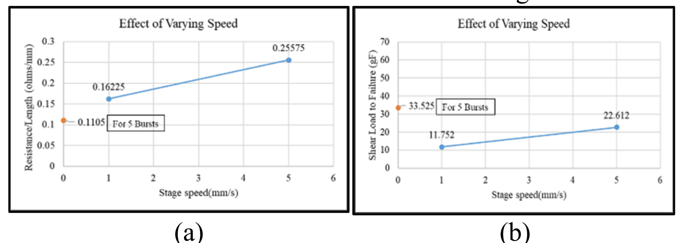

(a) (b)

Figure 30: Effect of Stage speed (a) Resistance/length (b) Shear load to failure

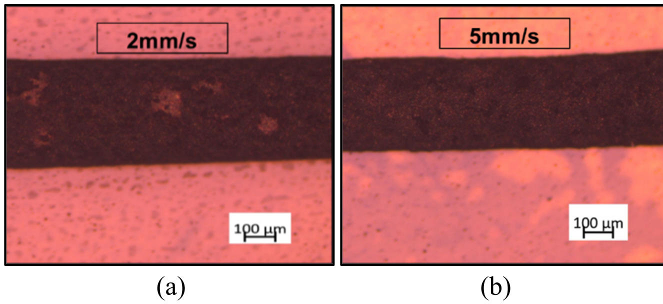

(a) (b)

Figure 31: Optical image of the surface at various Stage speed

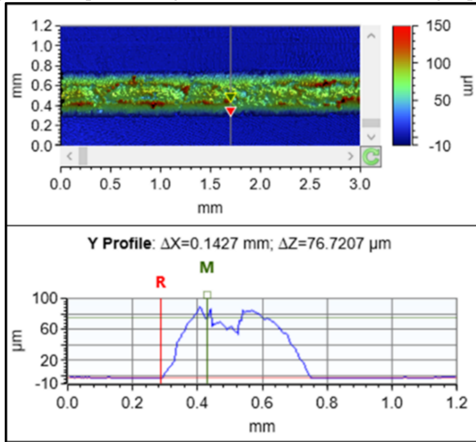

Figure 32: Trace profile and Height with samples sintered in burst mode

Figure 30, shows the effect of moving speed of the photonic curing bed as against the burst mode marked in orange dot on the graph. In the burst mode the stage just moves to the center and flashes the energy and returns back where as in continuous mode the flash recipe with the combination of the stage speed defines the percentage of overlap of flashes thus varying the amount of cure.

From Figure 31 and Figure 32 it can be concluded that the 2mm/s is over cured and 5mm/s is properly cured in terms of its surface profile but both are off in their electrical and mechanical values. 2mm/s due to over cure has cracks and pores which increases its resistance per unit length and reduces the shear load to failure value, whereas in case of the 5mm/s samples there are no cracks or popcorn failure as seen in Figure 33 but thus also shows that the electrical and mechanical properties are away from the desired values. Figure 32, shows the surface profile of the cured trace in the burst mode at 1000J and 0.7Hz. The height of the trace is 76.72µm and a width of 464.3µm. It can be seen that there is a drop in height in the center that is due to the popcorn failure.

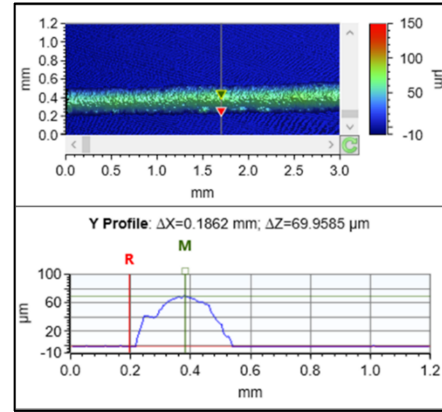

Figure 33: Trace profile and Height with one of the samples sintered in continuous mode

Figure 33, shows the surface profile of the cured trace in the continuous mode at 1000J and 0.7Hz at a stage speed of 5mm/s. The height of the trace is 69.96µm and a width of 328.8µm. It can be seen that there is no drop in height in the center thus giving a smoother surface.

e) Effect of Pre-heat

The samples sintered till this point had popcorn failure at various sintering parameters. The inconsistent trace profile may lead to varying performances with multiple component attachments thus to avoid the effect of trace deterioration we have also studied the effect of pre-heating the traces after printing in an conventional oven for a short duration for drying up the ink followed by photonic sintering. Figure 34 shows the effect of preheat on the resistivity of printed traces. The pre-heat time is 15 minutes. We see a dramatic difference in resistivity with the addition of pre-heat conditions. There is a decrease in resistivity of ~90 per cent. Figure 35 shows improved SLF value with preheat condition. The samples preheated at 60C for 15minutes tend to have a better SLF value as compared to other conditions. Figure 36 shows the change in trace width that can be seen due to addition of preheat condition.

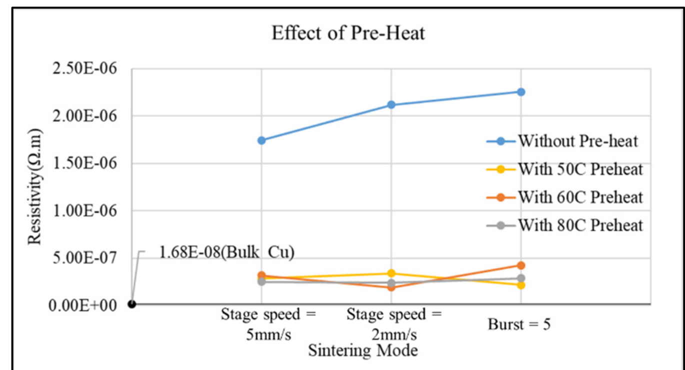

Figure 34: Effect of Pre-heat condition on resistivity

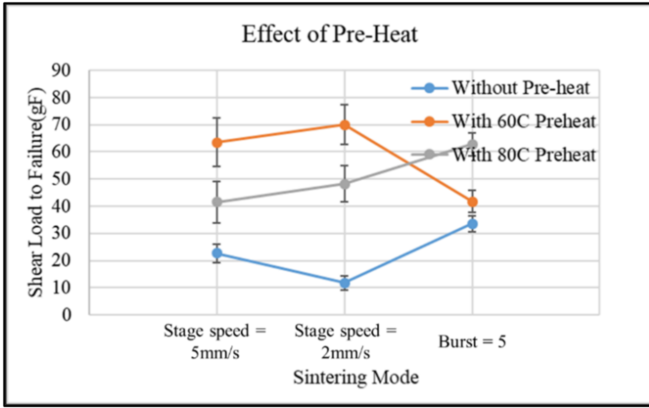

Figure 35: Effect of Pre-heat condition on shear load to failure value

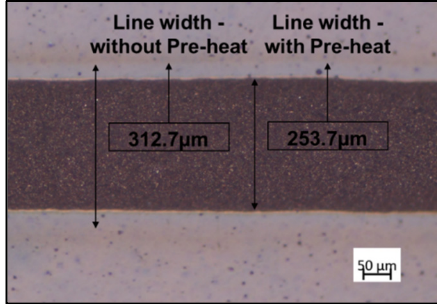

Figure 36: Effect of preheat on the trace profile

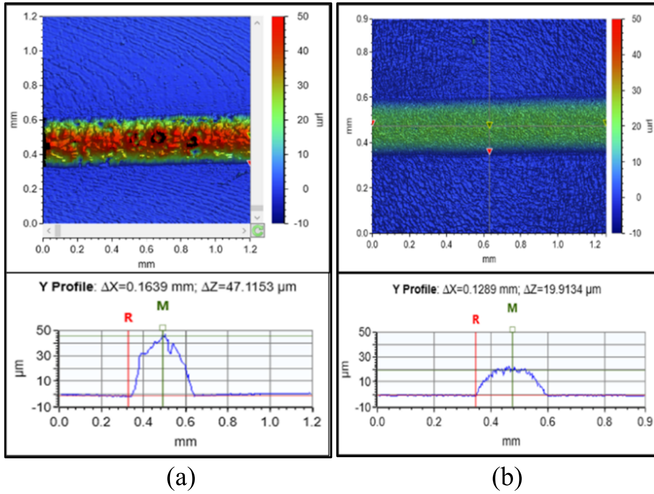

(a) (b)

Figure 37: Trace profile and Height with one of the samples sintered in continuous mode (a) without preheat (b) with preheat

There is a reduction in trace width of approximately 50µm due to preheat. The reason for this contraption in the profile probably needs to relate to the wetting of the surface mechanism. The reported value is an average of 5 samples. Figure 37 shows the effect of preheat on the profile geometry. The profile geometries are printed and sintered at same conditions to understand the effect of preheat in Figure 37. We do observe that the trace width and height reduces as well as the cross-sectional shape is more consistent without any popcorn type failure. Thus, introduction of preheat condition is beneficial for better mechanical and electrical properties from the results reported in Figure 34 and Figure 35.

B. Test results for design -2

Figure 38 - Figure 41, shows the stepwise process of the component attachment. Printing of copper followed by ECA printing and later component attachment with defined sintering conditions for each layer.

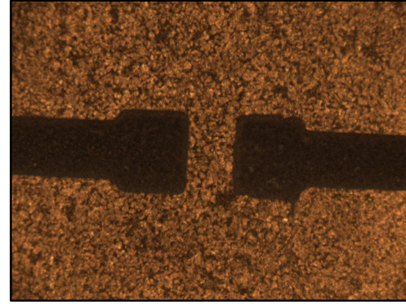
Figure 38: Image of the trace after sintering the Layer1

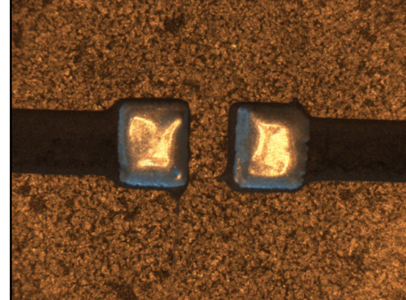
Figure 39: Image after the ECA printing before sintering

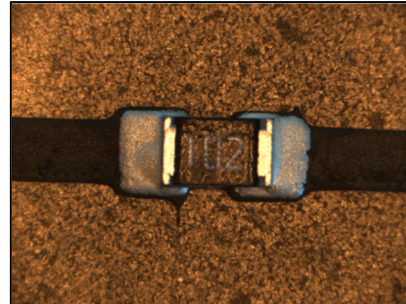
Figure 40: Image after the component attachment and sintering

The measurements seen in Figure 42 - Figure 44 are based on the Agilent 4192A LF impedance analyzer. The modules were measured at different frequencies to see the possible influence of the frequency on the interconnectivity. It can be noted that the calculated values are inside the tolerance range (marked by green dotted lines stating upper limit (UL) and lower limit (LL)) and can be verified with the black solid line representing the rated value in the graph. From the above findings, it can be assumed that we have been able to obtain a strong bond of interconnectivity to progress further.

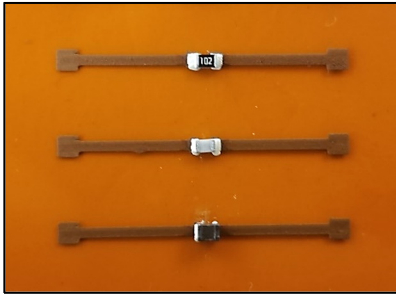

Figure 41: Components attached and notations mentioning each component position

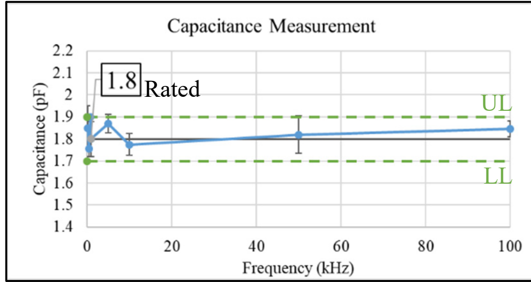

Figure 42: Measurement of the capacitor at various frequencies in comparison to rated value

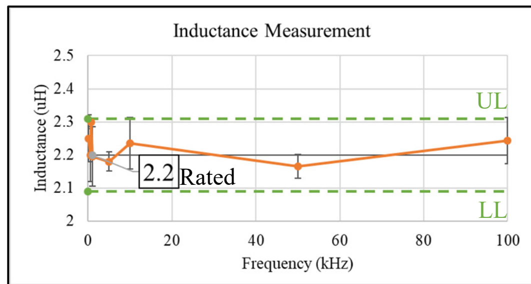

Figure 43: Measurement of the inductor at various frequencies in comparison to rated value

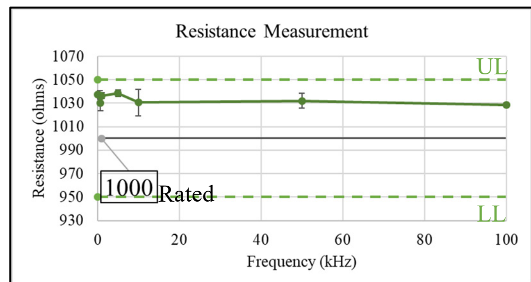

Figure 44: Measurement of the resistor at various frequencies in comparison to the rated value

1) LC-Filter

The discrete components used in the test of design 2 were different than the capacitors and inductors which are used in the test vehicle-3 because of the commercially bought LC filter. To test the variation in the rated values against the measured values we tested components before using in the actual test vehicle. From Figure 46 and Figure 47, it can be observed that there is variation in the rated (marked by a solid black line) and measured values but still, both the components are under their rated tolerance limit of 20% (marked with green dotted line).

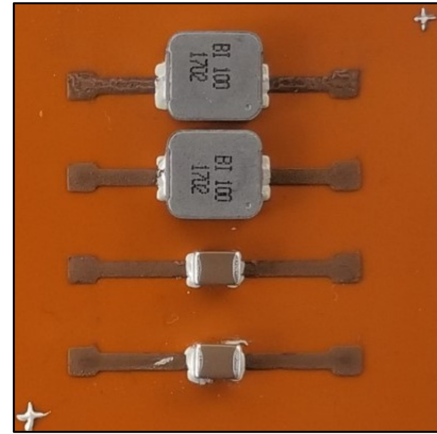

Figure 45: Image of components for testing

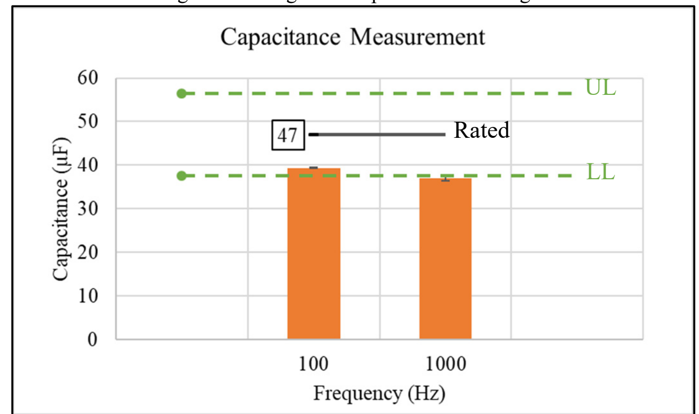

Figure 46: Measured Capacitance against the rated value

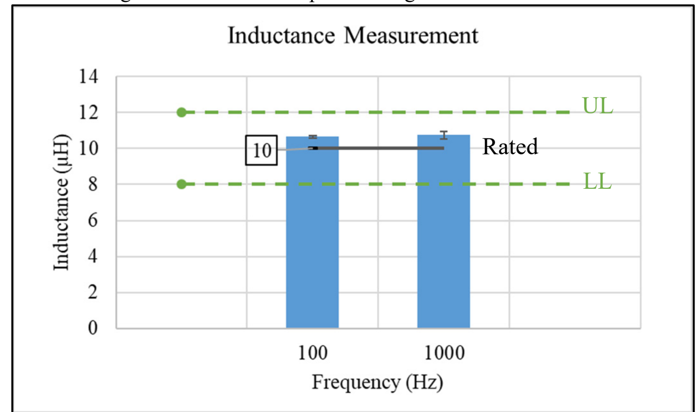

Figure 47: Measured Inductance against the rated value

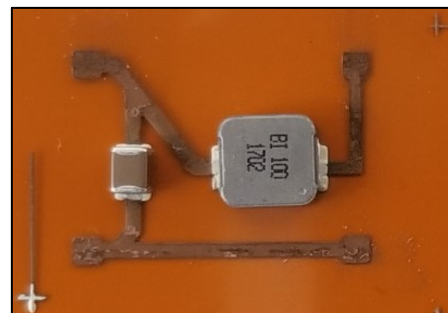

Figure 48: Printed flexible LC filter

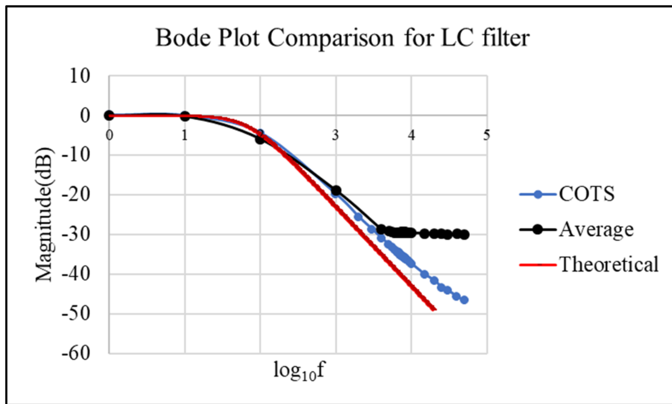

Figure 49: Bode plot comparison of the printed LC filter with the commercial LC filter

Figure 49 provides a comparison of the different flexible printed LC filters with the commercially purchased LC filter with the same capacitance and inductance. The output of the filters overlaps with the pattern. After frequency of 10^3 we do see some discrepancy, the major reason for this is that with increase in the frequency the capacitive and inductive reactance effects the output of the circuit thus causing the possible shift for the used components. At higher frequencies there is a shift observed in the measured filter output. [[16]]

IV. Summary and Conclusions

In this paper, we summarized the impact of various printing process parameters, such as ink pressure and printing speed, which affect trace geometry, viz. trace width and trace height, which is part of this work. Trace geometry knowledge plays a crucial role when printing an electronic circuit at a time when miniaturization is of the utmost importance. The research also looked at the effect of ink pressure and stage speed on the mechanical and electrical properties of the trace cross-section thus effecting the mechanical and electrical properties. The study was conclusive to state that the ink could be printed at 3mm/s and at a pressure of 15psi. Part two involves an overview of various parameters in photonic sintering, such as flash energy, flash time, frequency, burst mode, continuous mode with different stage speeds, which determines the resistivity and shear load to the failure value of the printed traces. The best condition will be to have the lowest resistance and the highest shear load to failure for stable and effective application. The preheat condition was of utmost important as it reduced the resistivity approximately 90% and also improving the SLF value. The third part of the analysis includes the attachment of the component using an ECA material. The key objective was to provide a stable ECA-copper curing condition in order to measure the reading of the device within the specified limits. For the application of the LC filter, it was necessary to maintain a combination of both, provided that it can be used later in bending, flexing and twisting situations. The components evaluated after an ECA connection show that they are well within the tolerance spectrum where the target was the establishment of interconnectivity with limited variance. The fourth section of the analysis focuses on evaluating the performance of the LC filter using the Bode plot. The efficiency analysis shows promising results and therefore it can be said that the development of the process study was carried out in order to obtain a working circuit and stands out to be a good qualification for the process study developed in this paper.

V. Acknowledgements

The project was sponsored by the NASA Marshall Space Flight Center at the NSF-CAVE3 Electronics Research Center at Auburn University.

VI. References

[1] A. Eshkeiti *et al.*, "Screen Printing of Multilayered Hybrid Printed Circuit Boards on Different Substrates," in *IEEE Transactions on Components, Packaging and Manufacturing Technology*, vol. 5, no. 3, pp. 415-421, March 2015.

[2] Tao, X., Koncar, V., Huang, T. H., Shen, C. L., Ko, Y. C., & Jou, G. T. (2017). How to make reliable, washable, and wearable textronic devices. *Sensors*, *17*(4), 673.

[3] Cantatore, E. (2013). Applications of organic and printed electronics. *A Technology-Enabled Revolution, Springer*.

[4] Church, K. H., Chen, X., Goldfarb, J. M., Perkowski, C. W., & LeBlanc, S. (2014). Advanced printing for microelectronic packaging. submitted for publication in IPC APEX Expo.

[5] Mypati, S., Docoslis, A., & Barz, D. P. (2020). Direct writing of liquids by micro dispensing: Stability and shape of laminar jets with high Froude numbers. Chemical Engineering Journal, 381, 122645.

[6] Chen, X., Church, K., Yang, H., Cooper, I. B., & Rohatgi, A. (2011, June). Improved front side metallization for silicon solar cells by direct printing. In 2011 37th IEEE Photovoltaic Specialists Conference (pp. 003667-003671). IEEE.

[7] Jin-Woo Park, Seong-Gu Baek, "Thermal behavior of direct-printed lines of silver nanoparticles", https://doi.org/10.1016/j.scriptamat.2006.08.032

[8] Seol-Min Yia, Ji-Hoon Leea, Na-Rae Kima, Sungil Ohb, Seonhee Jang, "Improvement of Electrical and Mechanical Properties of Ag Nanoparticulate Films by Controlling the Oxygen Pressure", 2010 ECS

[9] Chou, K. S., Huang, K. C., & Lee, H. H. (2005). Fabrication and sintering effect on the morphologies and conductivity of nano-Ag particle films by the spin coating method. Nanotechnology, 16(6), 779.

[10] Ko, S. H., Pan, H., Grigoropoulos, C. P., Luscombe, C. K., Fréchet, J. M., & Poulikakos, D. (2007). All-inkjet-printed flexible electronics fabrication on a polymer substrate by low-temperature high-resolution selective laser sintering of metal nanoparticles. Nanotechnology, 18(34), 345202.

[11] Lall, P., Narangaparambil, J., Leever, B., & Miller, S. (2019, May). Effect of Sintering Temperature on the Fatigue Life of Additively Printed Electronics During Cyclic Bending. In 2019 18th IEEE Intersociety Conference on Thermal and Thermomechanical Phenomena in Electronic Systems (ITherm) (pp. 189-197). IEEE.

[12] Son, Y. H., Jang, J. Y., Kang, M. K., Ahn, S., & Lee, C. S. (2018). Application of flash-light sintering method to flexible inkjet printing using anti-oxidant copper nanoparticles. *Thin Solid Films*, *656*, 61-67.

[13] Park, S. H., & Kim, H. S. (2014). Flash light sintering of nickel nanoparticles for printed electronics. *Thin Solid Films*, *550*, 575-581.

[14] Joo, S. J., Hwang, H. J., & Kim, H. S. (2014). Highly conductive copper nano/microparticles ink via flash light sintering for printed electronics. *Nanotechnology*, *25*(26), 265601.

[15] Hwang, H. J., Chung, W. H., & Kim, H. S. (2012). In situ monitoring of flash-light sintering of copper nanoparticle ink for printed electronics. *Nanotechnology*, *23*(48), 485205.

[16] Robles, U., Bustamante, E., Darshni, P., & Rumpf, R. C. (2019). High-Frequency Filters Manufactured Using Hybrid 3D Printing Method. *Progress In Electromagnetics Research*, *84*, 147-155.